

Supplementary Information:

Remarkable electron and phonon band structures lead to a high thermoelectric performance $ZT > 1$ in earth-abundant and eco-friendly SnS crystals

Wenke He,^{a,†} Dongyang Wang,^{a,†} Jin-Feng Dong,^b Yang Qiu,^c Liangwei Fu,^d Yue Feng,^d Yujie Hao,^{d,e,f} Guangtao Wang,^g Jinfeng Wang,^g Chang Liu,^{d,e,f} Jing-Feng Li,^b Jiaqing He,^{c,d} Li-Dong Zhao,^{a,*}

^aSchool of Materials Science and Engineering, Beihang University, Beijing 100191, China

^bState Key Laboratory of New Ceramics and Fine Processing, School of Materials Science and Engineering, Tsinghua University, Beijing 100084, China

^cPico Center, Materials Characterization and Preparation Center, Southern University of Science and Technology, Shenzhen 518055, China

^dDepartment of Physics, Southern University of Science and Technology, Shenzhen 518055, China

^eInstitute for Quantum Science and Engineering, Southern University of Science and Technology, Shenzhen 518055, China

^fShenzhen Key Laboratory of Quantum Science and Engineering, Shenzhen 518055, China

^gCollege of Physics and Materials Science, Henan Normal University, Xinxiang, 453007, China

†W. H. and D.W. contributed equally to this work.

*Corresponding author: zhaolidong@buaa.edu.cn

EXPERIMENTAL

Synthesis: High-purity elemental constituents of Sn (99.99%), S (99.999%) and Na (99.99%) were weighted in a stoichiometric ratio of $\text{Sn}_{1-x}\text{Na}_x\text{S}$ ($x = 0, 1\%, 2\%, 3\%$) and loaded into carbon-coated silica tubes under a glove box with nitrogen atmosphere. The tubes were evacuated and flame-sealed under pressure of $\sim 10^{-4}$ Torr. The outer tubes were used to prevent samples from oxidation because the inner tubes could break caused by high-temperature phase transition. The samples were slowly heated up to 873 K over 10 h and maintained for 40 h, and then heated up to 1223 K over 6 h and soaked for 10 h, and subsequently furnace cooled to room temperature. The obtained ingots (~ 14 g) were crushed into powder for X-ray diffraction and following crystal growth. The powders were charged into conical tubes and flame-sealed, and then loaded into vertical furnace, heated up to 1313 K at rate of 10 K min^{-1} and soaked for 10 h, subsequently cooled to 1073 K at a slow rate of 1 K h^{-1} and furnace cooled to room temperature. Finally, the $\text{Sn}_{1-x}\text{Na}_x\text{S}$ crystals with diameter of 13 mm and length of 30 mm were obtained, as shown in **Figure S1**.

Electrical transport properties: The obtained $\text{Sn}_{1-x}\text{Na}_x\text{S}$ crystals were cut into cuboid shaped samples along different axial directions with dimensions of $10 \text{ mm} \times 3 \text{ mm} \times 3 \text{ mm}$ and used for simultaneous measurement of the Seebeck coefficient and the electrical conductivity, which were measured by Cryoall CTA and Ulvac Riko ZEM-3 instruments under a low-pressure helium atmosphere from room temperature to 873 K. The samples were coated with a thin (~ 0.1 - 0.2 mm) layer of boron nitride (BN) to protect instruments. The uncertainty of the Seebeck coefficient and electrical conductivity measurement is within 5%.

Thermal Conductivity: The $\text{Sn}_{1-x}\text{Na}_x\text{S}$ ($x = 0, 1\%, 2\%, 3\%$) crystals were cut and polished into square-like samples of $6 \text{ mm} \times 6 \text{ mm} \times 2 \text{ mm}$ for thermal diffusivity measurements. The samples were coated with a thin layer of graphite to minimize errors from the emissivity of the material. The thermal conductivity was calculated from the equation $\kappa = DC_p\rho$, where the thermal diffusivity (D) was measured along the same direction as the electrical transport using the laser flash diffusivity method performed

on Netzsch LFA 457, the specific heat capacity (C_p) was obtained from reported values¹ and estimated with Dulong-Petit law, and the density (ρ) is determined by calculating the dimensions and mass of the sample and reconfirmed by Archimedes method. The thermal diffusivity data were analyzed using a Cowan model with pulse correction. Considering the uncertainties of D , C_p and ρ , the uncertainty of the thermal conductivity is estimated to be within 15%. The combined uncertainty for all measurements involved in the calculation of ZT is around 20%.

Hall measurements: Hall coefficients (R_H) were obtained by the Van der Paw technique under a reversible magnetic field of 0.52 T using Hall measurement system (8340 DC, Toyo Japan) at 300 K - 823 K. The samples with dimensions 8 mm \times 8 mm \times 0.5 mm was prepared and measured under argon gas atmosphere to avoid possible oxidation at high temperature. Carrier density (n_H) was calculated from $n_H = 1/(eR_H)$, and carrier mobility (μ_H) was calculated by the equation $\mu_H = \sigma R_H$, where σ is the electrical conductivity.

Transmission electron microscopy (TEM) analysis: The investigation of SnS sample by transmission electron microscope was performed with FEI Titan G2 Themis 60–300 Cube in both TEM and STEM imaging mode. The high resolution STEM images are acquired in the double corrected Titan system with the HAADF detector generally at 300 kV, unless specified otherwise. This condition allows high resolution that resolves each column of atoms without noticeable beam damage in the specimens. The images are acquired with a screen current of 0.05–0.1 nA, a convergence angle of ~ 18 mrad and a collection angle of 125–200 mrad. ABF STEM images are acquired simultaneously along with the HAADF STEM images with DF2 detector below the viewing screen with camera length equals to 58 mm. In addition, the EDX mappings are acquired with a screen current of 0.15–0.2 nA to gain enough EDX signals. The diffraction patterns (DPs) are acquired in TEM mode with 40 μm selected area (SA) aperture.

Thermogravimetric analysis (TGA) measurements: The thermogravimetric analysis (TGA) measurements were performed on Netzsch STA 449 F3 simultaneous thermal analyzer in crucible under a N_2 flow, in the temperature range from 300–900 K

with a rate of 5 K min⁻¹.

X-ray diffraction (XRD) and X-ray back-reflection Laue: Samples pulverized with an agate mortar were used for powder X-ray diffraction. The powder diffraction patterns were obtained with Cu K α ($\lambda = 1.5418 \text{ \AA}$) radiation in a reflection geometry on a diffractometer operating at 40 kV and 20 mA and equipped with a position-sensitive detector. The cleavage plane (100) of Sn_{1-x}Na_xS crystals were detected by X-ray back-reflection Laue to determine the in-plane (*b-c* plane) orientations. The crystals are placed according to their growth direction and their cleavage planes are facing to X-ray resource. The Laue patterns were obtained through collecting diffraction lines by a plate on a diffractometer operating at 18 kV and 18 mA.

Angle resolved photoemission spectroscopy (ARPES) measurements: The ARPES measurements were performed using a laboratory-based ARPES system consisting of a SPECS PHOIBOS 150 electron analyzer and a UVLS-600 UV lamp at a pressure lower than 1×10^{-9} mbar. The samples were cleaved in the ARPES chamber, yielding a clean, flat *b-c* surface which corresponds to the Y- Γ -Z plane in the Brillouin zone. The incident photon energy was 21.218 eV (He I), the spot diameter was about 500 micrometers. The energy resolution was kept at ~ 50 meV. Samples were found to be stable during a typical measurement period of ~ 20 hours, which is consistent with the TGA measurements, as shown in **Figure S6**.

Density functional theory (DFT) calculations: First-principles calculations within density functional theory (DFT) have been performed for SnS using the projector-augmented wave (PAW) method², as implemented in the Vienna Ab-initio Simulation Package (VASP)³. The exchange-correlation energy is treated in the generalized gradient approximation (GGA) Perdew-Burke-Ernzerhof (PBE)⁴. The spin-orbit coupling (SOC) was included in our calculations. Plane waves with an energy cutoff of 450 eV are used as the basis set for all the calculations. A Monkhorst-Pack Γ -centered $4 \times 12 \times 12$ k-point mesh is used for Brillouin zone sampling. All of the structures are fully relaxed until the maximum residual ionic force is below 0.01 eV/ \AA , and the total energy difference is converged to within 10^{-7} eV. Vibrational properties are calculated using $3 \times 3 \times 3$ SnS supercell contained 216 atoms with force constant

method by the Phonopy code. In the quasiharmonic DFT phonon calculations, the system volume is isotropically expanded by + 2 % from the relaxed equilibrium volume. The Grüneisen parameter (γ) is defined as

$$\gamma_i = -\frac{V \partial \omega_i}{\omega_i \partial V} \quad (2)$$

which characterizes the relationship between phonon frequency and volume change. The Grüneisen parameters provide an estimate of the strength of the anharmonicity in a compound. The minimum lattice thermal conductivity can be calculated using the approach developed by Cahill⁶:

$$\kappa_{min} = \left(\frac{\pi}{6}\right)^{1/3} k_B n^{2/3} \sum_i v_i \left(\frac{T}{\Theta_i}\right)^2 \int_0^{\Theta_i/T} \frac{x^3 e^x}{(e^x - 1)^2} dx \quad (3)$$

where v , Θ and n are the phonon velocity, Debye temperature and the number density of atoms, respectively.

Single parabolic band (SPB) model: The Pisarenko line calculated by the SPB model from Pisarenko formula:

$$S = \frac{k_B}{e} \left[\frac{2F_1(\eta)}{F_0(\eta)} - \eta \right] \quad (4)$$

where Fermi integral is

$$F_x(\eta) = \int_0^{\infty} \frac{\varepsilon^x}{1 + \exp(\varepsilon - \eta)} d\varepsilon \quad (5)$$

and reduced Fermi level is determined by carrier concentration,

$$n = \frac{(2m_d^* k_B T)^{3/2} F_{1/2}(\eta)}{2\pi^2 \hbar^3 r_H} \quad (6)$$

where Hall radius is

$$r_H = \frac{3F_{1/2}(\eta)F_{-1/2}(\eta)}{4 [F_0(\eta)]^2} \quad (7)$$

m_d^* is the density of state (DOS) effective mass, n is the hole density, k_B is the Boltzmann constant, \hbar is the reduced Planck's constant, e is the electronic charge and

T is the temperature. Here the DOS effective mass can be expressed as $m_d^* = (m_{k_x}^* m_{k_y}^* m_{k_z}^*)^{1/3} N_v^{2/3}$, where $m_{k_x}^*$, $m_{k_y}^*$ and $m_{k_z}^*$ are the calculated effective masses based on the first band of the valence band maximum (shown in **Figure 3(a)**), which are $2.24m_0$, $0.20m_0$ and $0.15m_0$, respectively, N_v is the degeneracy of hole pockets in Brillouin zone, which is 2 in our case. Therefore, the DOS effective mass of $0.64m_0$ is obtained in this work.

REFERENCES

1. Q. Tan, L. D. Zhao, J. F. Li, C. F. Wu, T. R. Wei, Z. B. Xing and M. G. Kanatzidis, *J. Mater. Chem. A*, 2014, **2**, 17302-17306.
2. P. E. Blöchl, *Physical Review B*, 1994, **50**, 17953-17979.
3. G. Kresse and J. Furthmüller, *Phys. Rev. B*, 1996, **54**, 11169-11186.
4. J. P. Perdew, K. Burke and M. Ernzerhof, *Physical Review Letters*, 1996, **77**, 3865-3868.
5. A. Togo, F. Oba and I. Tanaka, *Phys. Rev. B*, 2008, **78**, 134106.
6. D. G. Cahill, S. K. Watson and R. O. Pohl, *Physical Review B*, 1992, **46**, 6131-6140.

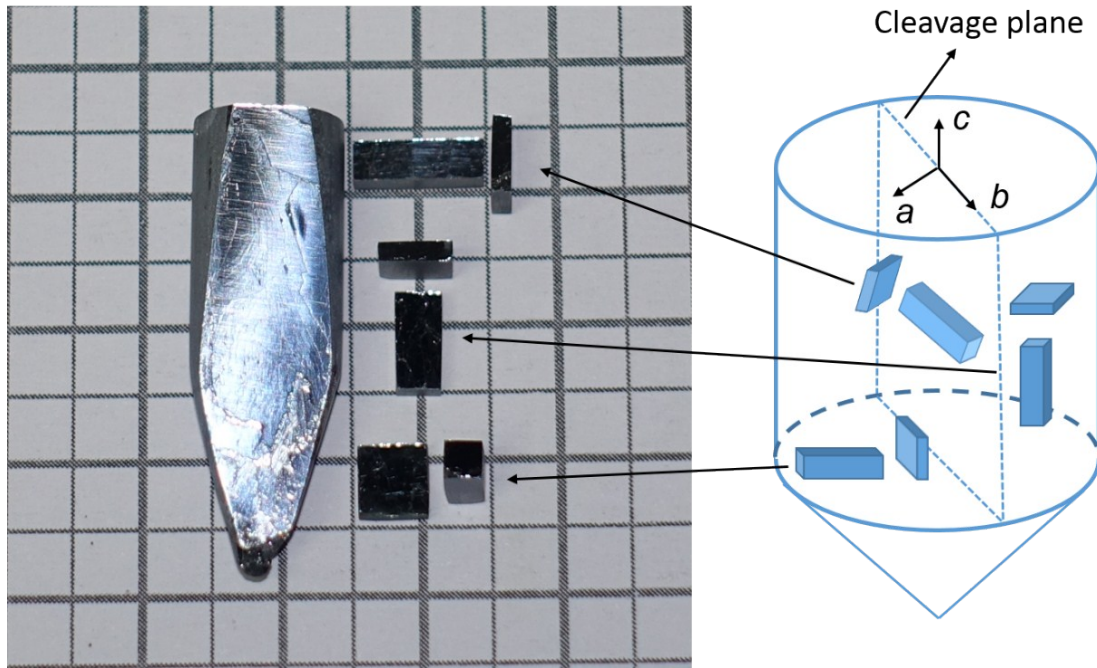


Figure S1. SnS crystal and samples along the three crystallographic directions for measurements: A typical crystal cleaved along (100) plane and the samples cut along the three crystallographic directions for thermoelectric properties measurements (left image), and corresponding diagram of cutting samples (right).

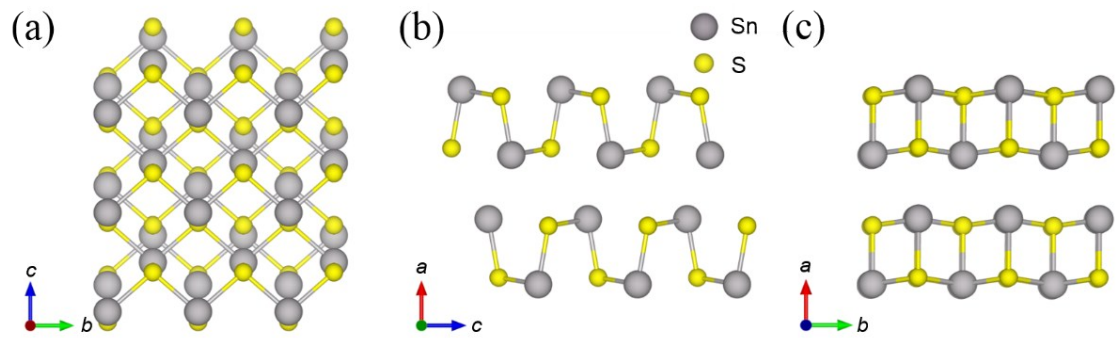


Figure S2. Crystal structure of SnS (*Pnma*): Crystal structures along the (a) *a* axis , (b) *b* axis and (c) *c* axis.

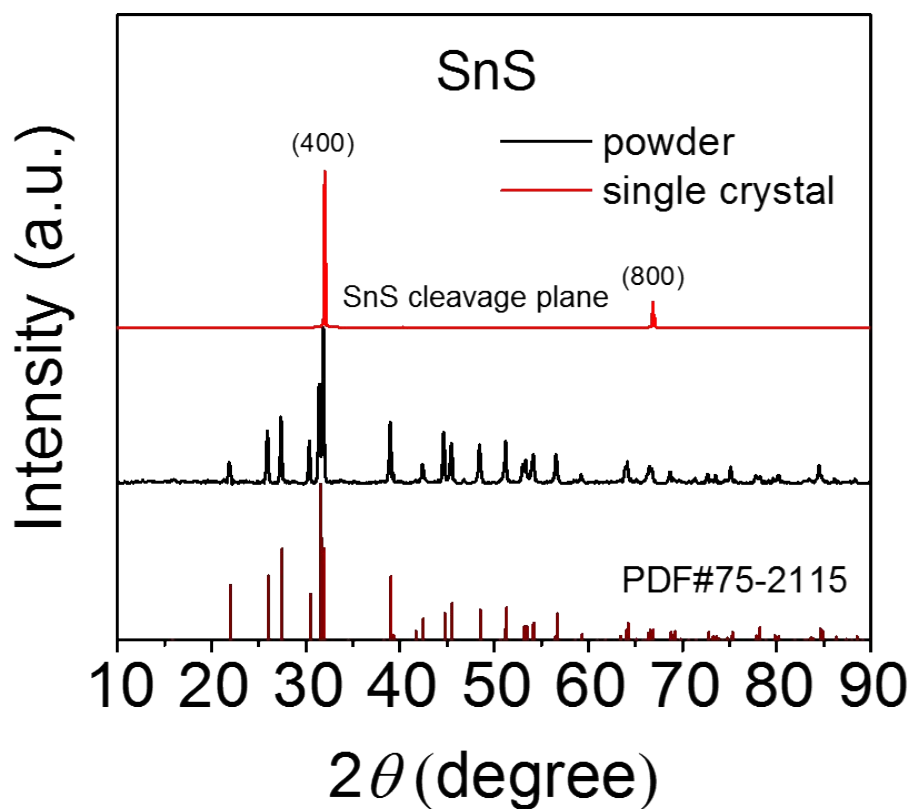


Figure S3. XRD patterns of SnS powder, SnS crystal on the cleavage plane and corresponding simulation pattern: The SnS powder diffraction pattern (black line) is consistent well with simulation pattern (PDF#75-2115). The (400) and (800) reflection planes indicate that the cleavage plane of SnS crystal is perpendicular to the a axes.

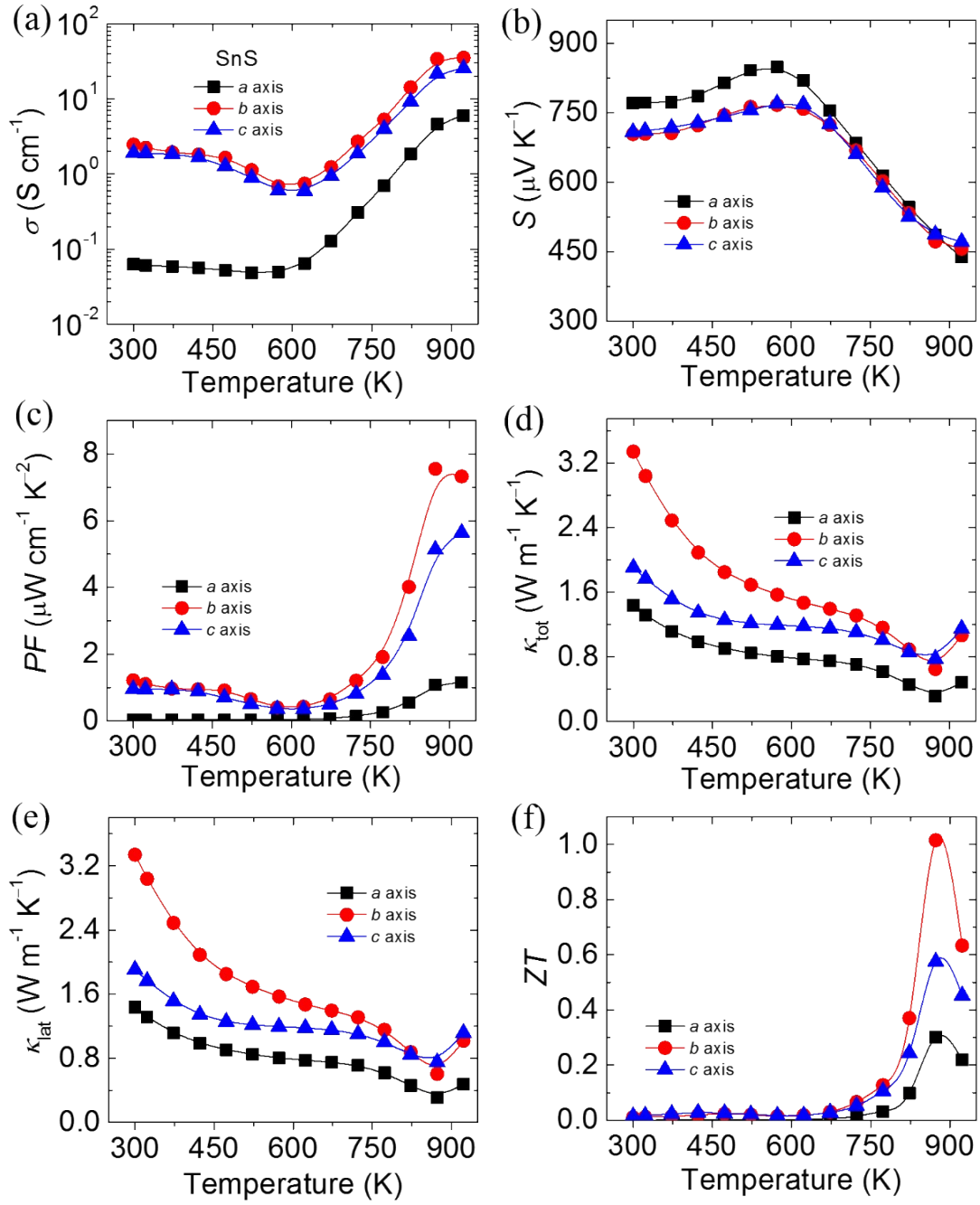


Figure S4. Thermoelectric properties as a function of temperature for undoped SnS crystals: (a) Electrical conductivity. (b) Seebeck coefficient. (c) Power factor. (d) Total thermal conductivity. (e) Lattice thermal conductivity. (f) ZT values.

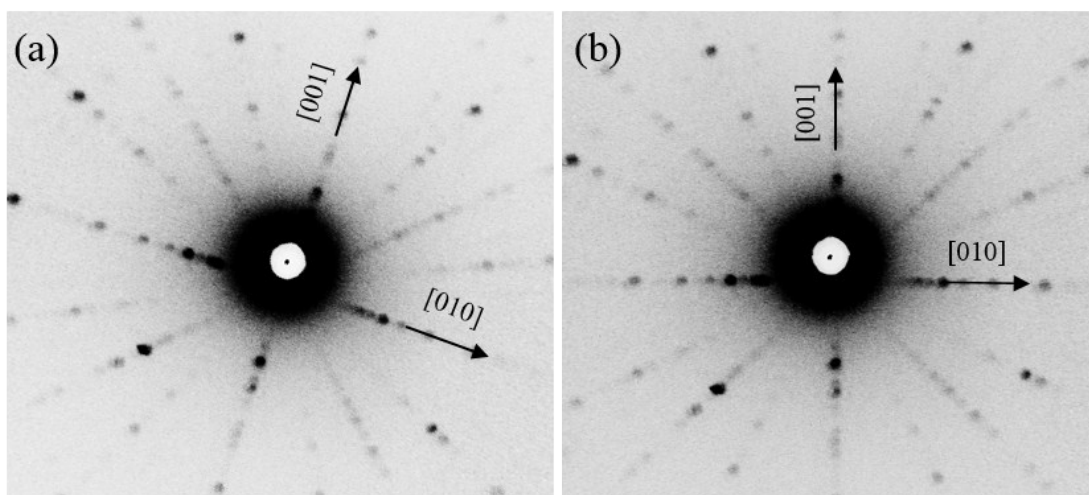


Figure S5. Laue pattern of SnS crystals on the cleavage plane of SnS crystals: (a) The Laue diffraction pattern of cleavage plane placed in according with the crystal growth direction. (b) The Laue diffraction pattern of SnS after rotating. $[010]$ and $[001]$ are the b and c axial orientations of SnS crystal, indicating a deviation of crystallographic axes.

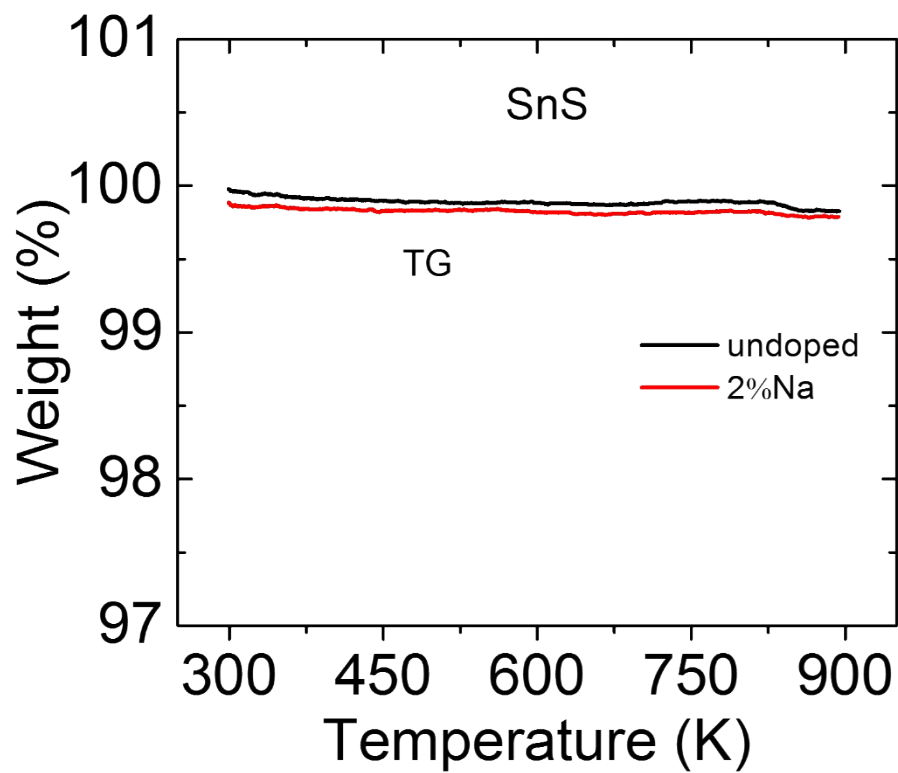


Figure S6. Thermogravimetric (TG) analysis of $\text{Sn}_{1-x}\text{Na}_x\text{S}$ ($x = 0, 2\%$) crystals: The results show that the mass of SnS crystals remain unchanged in the temperature range from 300 to 900K, indicating a good thermal stability of SnS crystals.

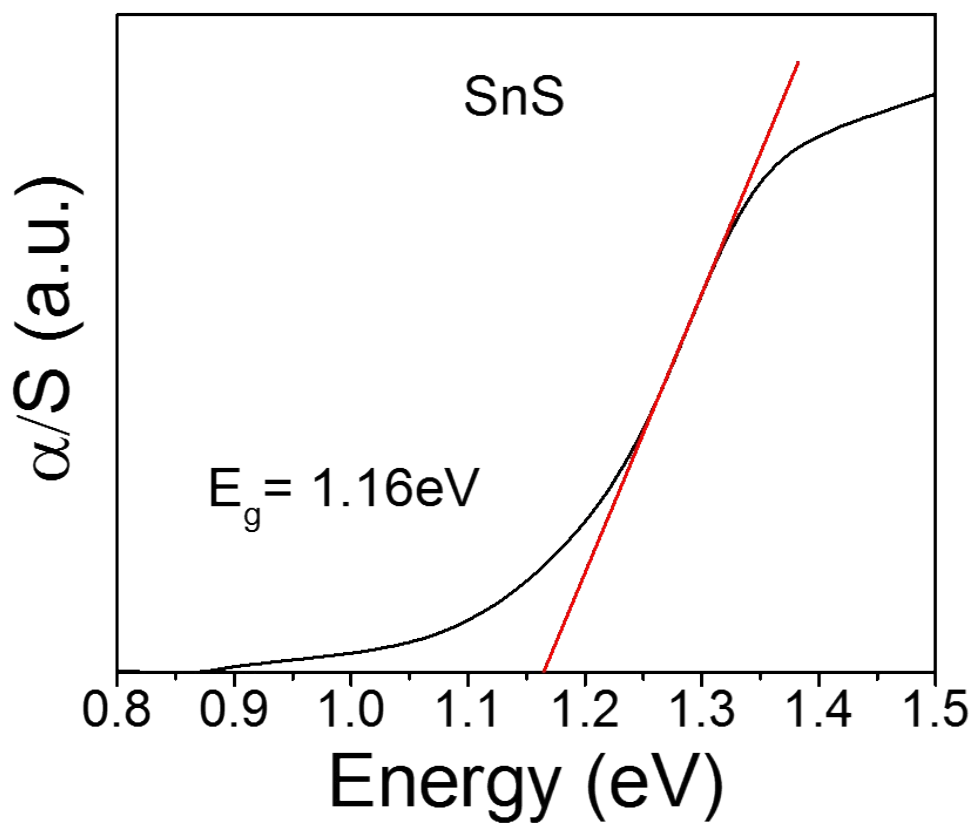


Figure S7. Bandgap of SnS at room temperature. Optical absorption spectrum (black line) and energy bandgap, indicating a bandgap of 1.16 eV at room temperature for in SnS.

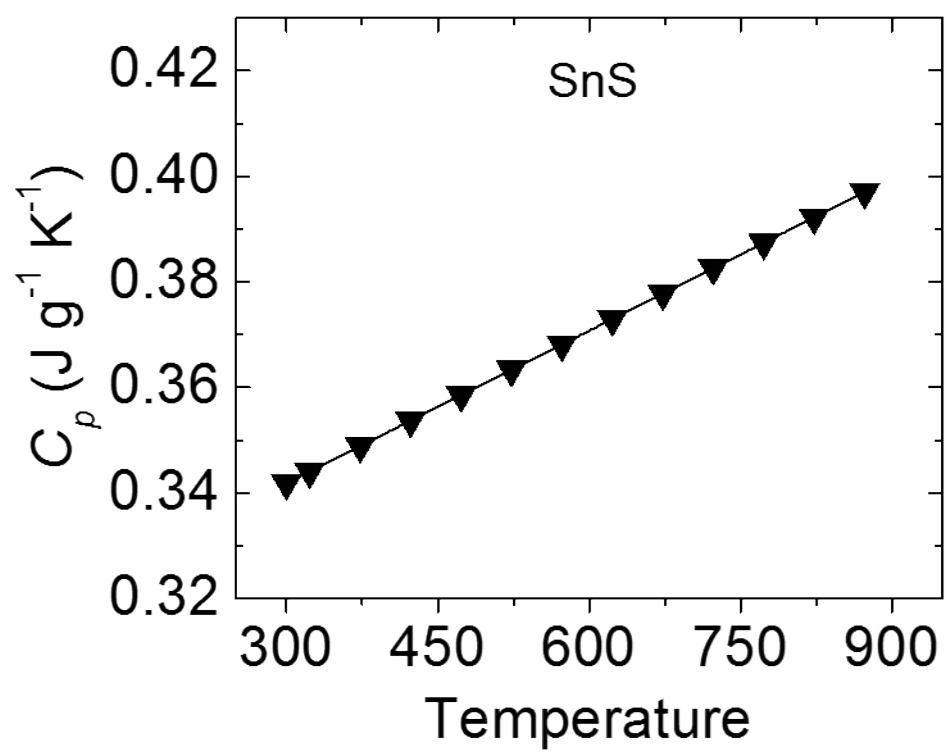


Figure S8. Specific heat capacity as a function of temperature for SnS.

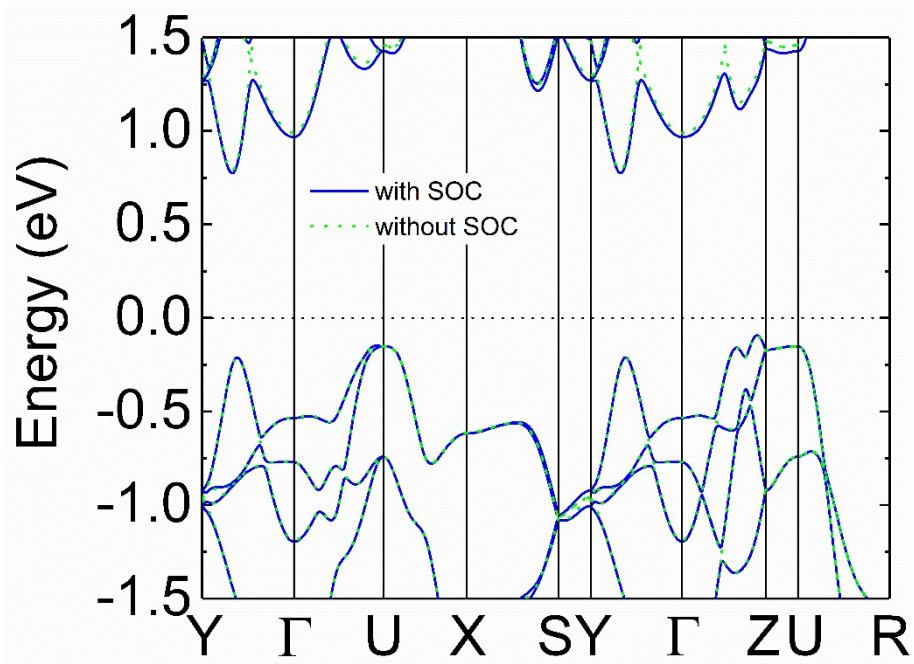


Figure S9. Band structures with SOC (solid line) and without SOC (dotted line) for SnS.

Table S1. Transverse (TA/TA') and longitudinal (LA) Debye temperature (Θ_D), phonon velocity (ν) and Grüneisen parameter (γ) along a , b and c axes: Values are calculated from phonon and the Grüneisen parameter dispersion (Figure 5(d)).

ΓX	Θ_D (K)	ν (m/s)	γ
TA	34.5	1475	5.13
TA'	35.2	1834	4.48
LA	39.7	2058	2.48
Average	36.5	1755	4.03
ΓY			
TA	71.2	1756	1.54
TA'	71.2	1712	2.76
LA	79.1	3538	1.47
Average	73.8	2089	1.92
ΓZ			
TA	44.9	2156	2.2
TA'	59.7	2505	2.04
LA	69.7	3431	1.93
Average	58.1	2599	2.06